Bioactive Materials 11 (2022) 118–129

Contents lists available at ScienceDirect

Bioactive Materials

journal homepage: www.keaipublishing.com/en/journals/bioactive-materials

Synergistic stimulation of surface topography and biphasic electric current promotes muscle regeneration

Indong Jun [a], Na Li [b], Jaehee Shin [c], Jaeho Park [d], Young Jun Kim [a], Hojeong Jeon [d], Hyuk Choi [c], Jae-Gu Cho [b], Byoung Chan Choi [e], Hyung-Seop Han [d,*], Jae-Jun Song [b,**]

[a] Environmental Safety Group, Korea Institute of Science & Technology Europe (KIST-EUROPE), Saarbrücken, 66123, Germany
[b] Department of Otorhinolaryngology-Head and Neck Surgery, Korea University College of Medicine, Seoul, 02841, Republic of Korea
[c] Department of Medical Sciences, Graduate School of Medicine, Korea University, Seoul, 02841, Republic of Korea
[d] Center for Biomaterials, Biomedical Research Institute, Korea Institute of Science & Technology (KIST), Seoul, 02792, Republic of Korea
[e] Laser Surface Texturing Group, AYECLUS, Gyeonggi-do, 14255, Republic of Korea

ARTICLE INFO

Keywords:
Topography
Electrical field stimulation
Femtosecond laser
Human myogenic precursor cell
Cell therapy

ABSTRACT

Developing a universal culture platform that manipulates cell fate is one of the most important tasks in the investigation of the role of the cellular microenvironment. This study focuses on the application of topographical and electrical field stimuli to human myogenic precursor cell (hMPC) cultures to assess the influences of the adherent direction, proliferation, and differentiation, and induce preconditioning-induced therapeutic benefits. First, a topographical surface of commercially available culture dishes was achieved by femtosecond laser texturing. The detachable biphasic electrical current system was then applied to the hMPCs cultured on laser-textured culture dishes. Laser-textured topographies were remarkably effective in inducing the assembly of hMPC myotubes by enhancing the orientation of adherent hMPCs compared with flat surfaces. Furthermore, electrical field stimulation through laser-textured topographies was found to promote the expression of myogenic regulatory factors compared with nonstimulated cells. As such, we successfully demonstrated that the combined stimulation of topographical and electrical cues could effectively enhance the myogenic maturation of hMPCs in a surface spatial and electrical field-dependent manner, thus providing the basis for therapeutic strategies.

1. Introduction

Cell therapy is a scientific approach that is expected to serve as a potential tool for skeletal muscle pathologies in the future mainly in the context of regenerative medicine [1–3]. A key strategy for this therapy is the transplantation of mononuclear cells in damaged muscle tissue [4]. The transplanted mononuclear cells fuse with the myofibers of the host tissue to form new myofibers, aiming to restore the defective muscle [5,6]. Autologous transplantation is one of the most representative clinical therapies but requires sacrificial healthy muscle tissue from patients and exhibits low-tissue integrity, including loss of function at the host site and host-site morbidity [7]. To overcome these limitations, myogenic progenitor cells (MPCs) have been used extensively in the field of cell-based regenerative medicine [8–10]. MPCs can be easily isolated, purified, and expanded *in vitro* without sacrificing their myogenic potential. They also possess enhanced differentiation capabilities in large multinucleated myotubes to provide a basic unit model of the mature skeletal myofiber [11]. However, it has been reported that the success rate is still low owing to the poor viability and low-therapeutic potential of the transplanted cells [12,13].

Cell cultures are essential tools extensively used in many fields of life sciences. Historically, cell cultures have been performed on culture dishes (commonly referred to as tissue culture polystyrene, TCP) owing to their low cost, optical clarity, and compatibility with cells [14]. However, commercially available culture dishes do not provide a structural environment similar to that observed physiologically. Isolated cells from the muscle tissue continually cultured on culture dishes are prone to lose their natural characteristics and often disrupt their potential for clinical transplantation [15]. Despite these limitations, many researchers continue to use commercially available culture dishes as the primary vessel. Specifically, the structural uniqueness of the skeletal

Peer review under responsibility of KeAi Communications Co., Ltd.
* Corresponding author.
** Corresponding author.
E-mail addresses: hyuhan@kist.re.kr (H.-S. Han), jjsong23@gmail.com (J.-J. Song).

https://doi.org/10.1016/j.bioactmat.2021.10.015
Received 21 July 2021; Received in revised form 27 September 2021; Accepted 14 October 2021
Available online 19 October 2021

Abbreviation list

3D	three-dimensional
BEC	biphasic electrical current
BEF	biphasic electric field
bFGF	fibroblast growth factor
bHLH	basic helix-loop-helix
BSA	bovine serum albumin
CTX	cardiotoxin
DMEM	Dulbecco's modified eagle's medium
DNA	deoxyribonucleic acid
EdU	5-ethynyl-2-deoxyuridine;
EGF	epidermal growth factor
EF	electrical field
FACS	fluorescence-activated cell sorting
FBS	fetal bovine serum
FITC	fluorescein 5-isothiocyanate
hMPC	human myogenic precursor cell
H&E	hematoxylin & eosin
HNA	anti-human nuclear antigen
HRP	horseradish peroxidase
HSP	heat shock protein
IGF	insulin-like growth factor
MCG	microcurrent generating
MHC	myosin heavy chain
MPC	myogenic progenitor cell
MRF	myogenic regulatory factor
MT	Masson's trichrome
NG	narrow gap;
PBS	phosphate buffer saline;
PVDF	polyvinylidene fluoride;
SEM	scanning electron microscope
SMA	smooth muscle actin
SSI	simultaneous stimulation induction culture platform
TA	tibialis anterior
TCP	tissue culture polystyrene
MHC	myosin heavy chain
OCT	optimal cutting temperature
U/V	ultraviolet;
WG	wide gap;
XPS	X-ray photoelectron spectroscopy

muscle requires biomimetic strategies to expedite the formation of organized myotubes from the orientation of differentiated cells [16–18]. Therefore, there is a need for an applied culture system that is capable of acquiring cells with therapeutic effects from an easily accessible platform that can manipulate cell fate and subsequently aid regeneration *in vivo*.

In this respect, many researchers agree that emulation of structural features is the preferred approach to enhance cell availability and promote transplanted cell maturation. Numerous scientific studies have investigated the enhanced myogenic cell fate by culturing cells on unique platforms with uniaxially aligned topographies using silicone, proteins, electrospun fibers, hydrogels, and metallic materials [19–23]. However, the uniaxially aligned topographies alone were insufficient for the efficient elevation of myogenesis and required a relatively long-term culture time for maturation to exert cell therapeutic effects. Muscle cells can sense different types of stimuli *in vivo*, such as chemical cues (e.g., growth factors and other soluble factors) and physical cues (e.g., elastic modulus, topography, and electrical signals) [24–26]. Electrical stimulation is imperative for maintaining the physiological functions of muscle cells (such as contractility and metabolism) for regenerative medicine applications [27–29]. Therefore, it is desired to emulate a co-stimuli-sensitive environment for muscle cells *in vitro* to determine the suitability of raw materials for cell therapy. Yang et al. reported the culturing of murine myoblasts on a patterned surface on an electrically conductive material surface [30]. They demonstrated that nanoscale directional surface structures could promote cell differentiation without electrical stimulation. Ko et al. reported that myogenic differentiation was promoted in C2C12 myoblasts cultured on aligned nanofibers obtained through high-speed electrospinning in electrical stimulation conditions [31]. Although cell fate control based on electrical stimulation and surface structure have been studied for a long time, research on the optimization of the spatial and electrical stimulations for better differentiation and maturation of human myogenic progenitor cells is ongoing.

In addition, although it is essential to obtain cells whose fate is precisely regulated in cell therapy, it is more critical to obtain cells in large quantities. It is well known that millions to billions of mature cells may be needed to provide a therapeutic effect [32,33]. Therefore, there is a need for a large-area culture platform to acquire large numbers of cells with controlled fate. In this study, we developed a simultaneous stimulation induction (SSI) culture platform that can simultaneously deliver both stimuli (surface topography and electrical stimuli) and present their versatile and simple uses as a universal culture platform for manipulating and acquiring high-quality human myogenic precursor cells (hMPCs) for cell therapy based on *in vitro* cellular and *in vivo* animal experiments. A method was implemented to establish biomimetic surface topographies on commercially available culture dishes using femtosecond laser texturing that can provide fast processing of single-step, large-scale operations. In addition, a detachable biphasic electrical current (BEC) system was used for electrical field stimulation. The main objective of this study was to determine the interactive effect of surface topography and electrical stimulation on adherent cell morphology and the orientations of differentiated myotube assemblies. We demonstrated that the SSI culture conditions regulate the directional myotube assembly and myogenic regulatory factors (MRFs) of hMPCs. Upon transplantation to an immunodeficient mouse model of cardiotoxin (CTX)-induced acute muscle damage, hMPCs that simultaneously experienced stimulations *in vitro* successfully contributed to muscle regeneration and angiogenesis *in vivo*. Our proof-of-concept approach can be utilized to harvest large numbers of myogenic progenitor cells with therapeutic properties. Collectively, our SSI platform may provide valuable fundamental results that allow us to advance cell therapy research.

2. Experimental section

2.1. Materials

Collagenase (type D), dispase, $CaCl_2$, and anti-myogenic factor 5 (MYF-5) were purchased from Sigma–Aldrich (St. Louis, MO, USA). Anti-heat shock protein-70 (HSP-70) and anti-CD31 (PECAM-1) were purchased from Cell Signaling Technology (Danvers, MA, USA). Anti-desmin, anti-Pax7, anti-laminin, anti-alpha smooth muscle actin (SMA), and chemiluminescent horseradish peroxidase (HRP) substrate were purchased from Abcam (Cambridge, MA, USA). Unless stated otherwise, all media and reagents were purchased from Thermo–Fisher Scientific (Waltham, MA, USA).

2.2. Isolation and cultivation of myogenic precursor cells

The infrahyoid muscles are surgically accessible in patients who undergo routine thyroidectomies [34,35]. Muscle biopsies were

obtained from human infrahyoid muscles in patients who underwent thyroid surgery at the Korea University Guro Hospital. The protocol used to obtain muscle biopsies from the consenting patients was approved by the Korea University Medical Center Institutional Review Board (No. 2019GR0246). Obtained human muscle tissue was washed and minced intensively using a scissors and digested in a mix of collagenase (type D) (0.75 U/ml), dispase (1.2 U/ml), and $CaCl_2$ (2.5 mM) in Dulbecco's modified eagle's medium (DMEM) for 1 h at 37 °C. hMPCs were cultured using conditioned media as described previously [36]. Briefly, after digestion, the enzymatic reaction was terminated in a culture medium (DMEM/F12 supplemented 20% fetal bovine serum (FBS), 10^{-6} M dexamethasone, 10 ng/ml epidermal growth factor (EGF), 1 ng/ml basic fibroblast growth factor (bFGF), 10 ng/ml insulin-like growth factor (IGF), and 1% penicillin–streptomycin), and filtered through a strainer with pore sizes of 100 μm and 70 μm, respectively. After centrifugation, the pellet was resuspended in a culture medium. As primary cultures from muscle tissue typically contain fibroblasts in addition to myoblasts, we conducted a preplating step to improve the purity and quality of primary muscle precursor cells. The medium was changed every 3 days, and the isolated hMPCs were characterized, as shown in Supporting Information (S1). For all experiments, hMPCs between passages 4 and 6 were used.

2.3. Laser texturing of commercially available culture dish ("surface topography")

A femtosecond laser (S-Pulse HP, Amplitude, Pessac, France) was used to create groove patterns on the surfaces of the culture dishes. The wavelength of the laser was 515 nm, pulse duration was 400 fs, and repetition rate of the laser pulse was 500 kHz. A laser texturing parametric study on the culture dishes (Corning, NY, USA) was conducted to select a parameter (pulse energy and speed of process) that produces the desirable characteristics of groove/ridge patterns (Supporting Information S4–5 and S13). After the laser texturing, samples were immersed in phosphate buffer saline (PBS) solution and sonicated for 5 min for cleaning.

2.4. Microcurrent generating chamber system ("biphasic electric current")

We used a custom-made detachable microcurrent generating (MCG) chamber to stimulate the hMPCs during the biphasic electric field (EF) stimulation period. The MCG chamber which delivers constant current through a constant-current circuit using the resistance sensor was composed of a bottom plate made of duralumin and platinum-coated electrodes and was covered with a lid. The MCG chamber specifications were described in our previous study [37]. The MCG chamber was adjusted to apply the BEF in the range of 50–500 mV/mm (duration of current 500 ns and frequency: 200 pulses/s). BEF was controlled by the ATmega128 microcomputer unit (Mouser Electronics Inc., Kwun Tong, KL, Hong Kong, China) to maintain atmospheric conditions. Atmega-128 was controlled by an IAR Embedded Workbench (IAR Systems, Uppsala, Sweden) within the range of 0–16 MHz. The output voltage was calibrated using an oscilloscope (model DSO6014A, Agilent Technologies, Santa Clara, CA, USA) and a picoammeter (model 6485, Keithly, Cleveland, Ohio, USA). For cell cultures, the cellular environment was maintained at a temperature of 36.5 ± 0.5 °C, with a humidity of 70%, and a CO_2 concentration of 5% in the atmosphere.

2.5. Surface characterization of laser-textured cell culture dishes

The morphologies of the laser-textured culture dishes were investigated using a scanning electron microscope (SEM, Inspect F50, FEI Company, Hillsboro, OR, USA). The samples were mounted onto stubs and coated with gold with the use of a sputter coater for 5 min. The laser-textured cell culture dishes were examined with the use of a three-dimensional (3D) laser confocal scanning microscope (OLS5000, Olympus, Japan). Elemental compositions that might have changed owing to laser ablation on the surface were investigated using X-ray photoelectron spectroscopy (Sigma Probe, Thermo VG Scientific, UK) to identify the differences before and after laser texturing.

2.6. Cell viability

To confirm the viability of the hMPCs on laser-textured cell culture plasticware in a detachable MCG chamber system, the cells were seeded at a density of 1×10^4 cells/cm^2, cultured in growth media for 12 h, and stained with the LIVE/DEAD™ viability/cytotoxicity kit. The cells were visualized with the use of confocal laser scanning microscopy (LSM 700, Carl Zeiss, Germany). Quantitative cell viability was evaluated for 12 h with a 4-[3-(4-iodophenyl)-2-(4-nitrophenyl)-2H-5-tetrazolio]-1,3-benzene disulfonate EZ-cytox cell viability assay kit (WST-1, ITSBIO, Seoul, Korea). Enzymatic activity was measured at an absorbance of 440 nm with the use of an ultraviolet (U/V) spectrophotometer (TECAN, Männedorf, Switzerland).

2.7. Characterization of adherent cells with simultaneous stimulation

Cell nuclei and actin filaments were counterstained with Hoechst 33258 and rhodamine-phalloidin, respectively. Cells cultured on laser-textured culture dishes were fixed with 4% paraformaldehyde for 20 min and then permeabilized in cytoskeleton buffer (0.5% Triton X-100 in PBS). After permeabilization, the hMPCs on the laser-textured culture dishes were blocked by incubating them with 5% FBS and 0.1% Tween-20 in PBS. They were subsequently incubated with rhodamine-phalloidin and 4′6′-diamidino-2-phenylindole (DAPI) for staining the cytoskeletal structure and nuclei, respectively. More than five DAPI-stained images were captured per sample and were scored for nuclear orientation and aspect ratio, which was calculated with the use of the software ImageJ (National Institutes of Health, Bethesda, MD, USA). The aspect ratio of the nuclei was determined by dividing the short-axis length (width) by the long-axis length at the same magnification. The orientation angle of individual nuclei was defined as the angle between the major axis of the adherent nuclei and the direction of the underlying groove patterns on the laser-textured culture dishes. Finally, we plotted it using the polar stacked column plot method with the use of the software Origin 2019 (OriginLab Corporation, Northampton, USA). To evaluate proliferation at 24 h, hMPCs were incubated with 5-ethynyl-2-deoxyuridine (EdU, 10 μM) in a growth medium for 2 h, and then sequentially dissociated using StemPro™ Accutase™ Cell Dissociation Reagent. Fixation, saponin-based permeabilization, and the EdU incorporation into deoxyribonucleic acid (DNA) were detected using the Click-iT EdU Alexa Fluor 488 flow cytometry assay kit. Fluorescence-activated cell sorting (FACS) analysis was performed with the use of the ZE5™ cell analyzer (Bio-Rad Laboratories, Hercules, CA, USA). Unstained hMPCs were used to define the FACS gating parameters. Qualitative and quantitative analyses of EdU-positive nuclei were performed using the FCS Express software (De Novo™ software, Glendale, CA, USA). To measure the DNA content at designated time points (1, 3, and 5 days), hMPCs were lysed in a radioimmunoprecipitation assay (RIPA) lysis buffer. The DNA content was quantified with the use of a Quant-iT™ PicoGreen™ dsDNA assay kit and a spectrofluorometer at the excitation and emission wavelengths of 480 nm and 520 nm, respectively.

2.8. Identification of the satellite cell-specific cell-surface markers

Cultured hMPCs were fixed with 4% paraformaldehyde for 30 min and then permeabilized with a cytoskeleton buffer for 20 min. Nonspecific binding was blocked with 1% bovine serum albumin (BSA) in PBS for 1 h. Samples were sequentially incubated with anti-Pax7 (1:100) for 1 h and the fluorescein 5-isothiocyanate (FITC) goat anti-

mouse immunoglobulin G for 1 h. Finally, the hMPCs were treated with a mounting medium which contained DAPI (Vector Labs, Oxfordshire, UK). Immunostaining of Pax7 in hMPCs was observed using confocal laser scanning microscopy. For the FACS analysis of cultured hMPCs, approximately 10^5 cells were collected and then fixed with 4% paraformaldehyde. The cells were then incubated with anti-Pax7 in 1% BSA in PBS. After primary antibody incubation, the hMPCs were washed with PBS three times and reconstituted in PBS. FACS analysis was performed using the ZE5™ cell analyzer. Unstained hMPCs were used to define the FACS gating parameters.

2.9. Protein expression depending on the stimulus

Protein lysates from hMPCs were isolated with the RIPA buffer supplemented with a 0.1% protease inhibitor cocktail 48 h after the external stimulus. The cell extract (which contained 20 μg of protein) was separated by sodium dodecyl sulfate-polyacrylamide gel electrophoresis (SDS-PAGE). After blotting onto a polyvinylidene fluoride (PVDF) membrane (Bio-Rad Laboratories, Hercules, CA, USA), the membranes were probed with HSP-70 and β-actin, followed by incubation with HRP-conjugated secondary antibodies. Immunoblots were visualized using a chemiluminescence imaging system (Azure 600, Azure biosystems, Dublin, CA, USA) with enhanced chemiluminescence reagent. With the use of ImageJ, the relative intensity of HSP-70 was quantified and compared with the expression of β-actin, which was then normalized by the value derived from hMPCs that were cultured on a flat surface without EF stimulus (Flat).

2.10. Characterization of early myogenic differentiation depending on the stimulus type

To induce myogenic differentiation of hMPCs, cells were seeded on cell culture dishes (density of 5×10^4 cell/cm^2) and cultured in growth media for 24 h. The media were then replaced with differentiation media (MEM alpha supplemented with 2% horse serum and 1% penicillin–streptomycin) and cultured for an additional 14 days. For immunostaining for early myogenic differentiation markers (MYF5 and MyoD), the cultured hMPCs (for 3 days) were fixed, permeabilized, incubated with anti-MYF5 and anti-MyoD, and visualized via confocal laser scanning microscopy. The quantification of MyoD-positive nuclei was performed using ImageJ. For the FACS analysis of cultured hMPCs (after 3 days with the use of differentiation media), approximately 10^5 cells were collected and then fixed in 4% paraformaldehyde. The cells were then incubated with anti-MYF5 in 1% BSA in PBS. After primary antibody incubation, the hMPCs were washed with PBS three times and reconstituted in PBS. FACS analysis was performed in the ZE5™ cell analyzer. Unstained hMPCs were used to define the FACS gating parameters. Protein lysates from differentiated hMPCs at 3 days were isolated with the RIPA buffer. The cell extract that contained 20 μg of protein was separated by SDS-PAGE. After blotting onto the PVDF membrane, the membranes were probed with MYF5 and β-actin, followed by incubation with HRP-conjugated secondary antibodies. Immunoblots were visualized with the use of a chemiluminescence imaging system with enhanced chemiluminescence reagent. Using ImageJ, the relative intensity of MYF5 was quantified compared with the expression of β-actin, which was then normalized by the value derived from hMPCs that were cultured on a flat surface without an EF stimulus (Flat).

2.11. Characterization of late myogenic differentiation depending on stimulus type

For immunostaining for late myogenic differentiation markers, the hMPCs were respectively cultured at 7 days and 14 days for myogenin and myosin heavy chain (MHC); fixed, permeabilized, and incubated with anti-myogenin and anti-MHC; and visualized using confocal laser scanning microscopy. Quantification of the myogenin- and MHC-positive nuclei was performed using ImageJ. More than five representative MHC-images per group were scored for the myotube distribution using the ImageJ software. The distribution of the myotube orientation was analyzed in a similar manner according to the degree of the long axis of the fused myotube. A value of 0° indicated that the myotubes had assembled in the anisotropic direction associated with the microgrooves on the laser-textured cell culture dishes. We plotted the results using the polar stacked column plot method with Origin 2019. For the FACS analysis of cultured hMPCs for 14 days in differentiation media, approximately 10^5 cells were collected and then fixed (4% paraformaldehyde). The cells were then incubated with FITC conjugated anti-MHC in 1% BSA in PBS. After primary antibody incubation, the hMPCs were washed with PBS three times and reconstituted in PBS. FACS analysis was performed in the ZE5™ cell analyzer. The unstained hMPCs were used to define the FACS gating parameters.

2.12. Intramuscular cell transplantation

The animal experiment was approved by the Institutional Animal Care and Use Committee (IACUC) of Korea University (No. KOREA-2019-0128). One day before cell transplantation, 8-week old immunodeficient mouse models (BALB/c mice, Orient Bio Inc, Korea, $n = 10$) were anesthetized with isoflurane, and tibialis anterior (TA) muscle damage was induced following the injection of 10 μL of 100 μM CTX (Merck KGaA, Germany) with the use of a 26 s gauge Hamilton syringe. Before transplantation, the hMPCs had been cultured for 48 h with or without external stimuli in growth media conditions. Subsequently, hMPCs were harvested and dissociated to a single-cell suspension by the StemPro™ Accutase™ cell dissociation reagent. The cells were then washed with PBS, centrifuged, and resuspended in saline solution at a density of 1.5×10^5 cells in 20 μL. The hMPCs were then injected into the right TA muscles, whereas the left TA muscles received the same volume of saline (controls). Two weeks post-transplantation, the mice were euthanized, and the TA muscles were harvested and either fixed for immunohistochemistry or dissociated for flow cytometry analysis.

2.13. Immunohistochemistry

The TA muscles were extracted and fixed in 4% paraformaldehyde for 24 h at 4 °C. Muscle tissues were then transferred to a 20% sucrose solution at 4 °C. They were then embedded and frozen in paraffin or optimal cutting temperature (OCT) and stored at −80 °C prior to further processing. The paraffin-embedded tissues were stained with hematoxylin and eosin (H&E, BBC Biochemical, WA, USA) and Masson's trichrome (MT, Polysciences, Inc., PA, USA) to identify muscle degeneration and fibrosis in the transplanted cells in the defect region. Frozen tissues were sectioned and mounted at a thickness of 10 μm. The tissue sections were rehydrated, blocked, and permeabilized with blocking solution (20% FBS and 1% Triton-X100 in PBS) overnight at 4 °C. A primary antibody was added to the slides and incubated overnight at 4 °C. Secondary antibody solutions were added to the slide and incubated for 1 h at 20 °C. The slides were then mounted and visualized by confocal laser scanning microscopy. Primary antibodies used in this experiment were anti-human nuclear antigen (HNA), anti-desmin, anti-laminin, anti-myosin heavy chain (Myosin or MYH), anti-alpha SMA, and anti-PECAM. Secondary staining was performed using goat anti-rabbit 488, goat anti-mouse 488, goat anti-rabbit 647, and goat anti-mouse 647.

2.14. Statistical analysis

All quantitative results were obtained from triplicate samples. Data were expressed as means ± standard deviations, and analyses were conducted with the use of the GraphPad Prism software (version 8.0, GraphPad Software, San Diego, CA, USA). Statistical analysis was

performed with the use of analysis of variance and Tukey's honestly significant difference test. P values < 0.05 were considered to be statistically significant.

3. Results and discussion

3.1. Characteristics of isolated human myogenic precursor cell (hMPCs)

Myogenic precursor cells are referred to as a pool of undifferentiated cells, such as donor-derived satellite and stem cells [38,39]. We identified that freshly isolated hMPCs could express Pax-7 (established marker for satellite cells), Desmin (the earliest marker for muscle), and CD44 (a stem cell marker) (Supporting Information S1). To confirm the myogenic properties of the hMPCs, cells were grown to confluence and induced to differentiate by replacing the growth medium with a differentiation medium (Supporting Information S2). After 14 days in the differentiation medium, hMPCs demonstrated the capacity to fuse and form multinucleated myotubes. A promising strategy for improving the treatment of damaged muscle tissue involves the induction of regeneration by integrating transplanted cells [38,40]. Consistent with the previous reports, we demonstrated cell proliferation, differentiation, and significant functional decline as a function of the passage number (Supporting Information S2–3 and S10). It is preferable to use early-passage cells for cell therapy, but it is well known that millions to billions of mature cells may be needed to provide therapeutic benefits. In addition, although it is vital to obtain cells whose fate is precisely controlled in cell therapy, it is more critical to obtain cells in large quantities. Therefore, there is a need for a large-area culture platform that can acquire a large number of cells with controlled fate and therapeutic potency. That is why we selected a commercially available plastic culture dish as the primary vessel. In other words, it is a priority to develop universal and innovative cell culture platforms that can expand a large number of cells from freshly isolated cells while maintaining their function. In this context, noncontact femtosecond laser processing and detachable electrical field stimulation systems in commercially available plastic culture dishes may represent a universal and innovative strategy for cell therapy that can overcome current translational clinical entry limits. Therefore, the approach of combining typography and electric fields in a convenient platform that can induce preconditioning therapeutic cells for muscle regeneration may be advantageous (Fig. 1).

3.2. Characteristics of the laser-textured culture dishes

Laser texturing of biomaterials enables the control of cellular behavior, particularly cell morphology [41,42]. The use of a femtosecond laser technique enables the rapid fabrication of precise patterns on the surface of a wide range of biomaterials. A femtosecond laser with short laser pulse durations (10^{-15} s) can fabricate pattern grooves with the minimal heat-affected zone [43,44]. It is possible to fabricate various anisotropic patterns and scales on culture dishes with the use of laser processing parameters, such as speed, energy pulse, number of pulses, and interval ablated lines (Supporting Information S4–5). Among these conditions, we performed subsequent experiments by identifying the laser conditions on culture dishes that could most effectively provide the orientation of adherent hMPCs without causing cell damage (Supporting Information S6). Fig. 2a–d depicts the surfaces of each culture dish subjected to laser fabrication with SEM and 3D microscopy. 3D laser confocal scanning microscopy confirmed the formation of microscale groove patterns with a defined width (11.66 ± 0.59 μm), depth (2.78 ± 0.11 μm), and roughness (0.72 ± 0.001 Ra, μm). Additionally, the XPS spectra of the laser-textured culture dish yielded a similar characteristic peak that corresponded to C 1 s (288 eV) and O 1 s (533 eV), in comparison with the culture dish without laser processing (Fig. 2e). The surface patterns of the culture dishes obtained using the femtosecond laser were designated as a narrow gap (NG) and wide gap (WG) and corresponded with the spacings between the groove ablated by the femtosecond laser at 35.36 ± 0.79 and 86.07 ± 0.94 μm. Flat refers to the culture dish without laser processing (used as a control group). It is believed that surface energy substantially influences wettability, and different spatial structures of laser-textured culture dishes have been reported to influence the wetting behavior of materials significantly [45]. There was a significant difference in the contact angle according to the surface characteristics of the laser-textured culture dishes. The

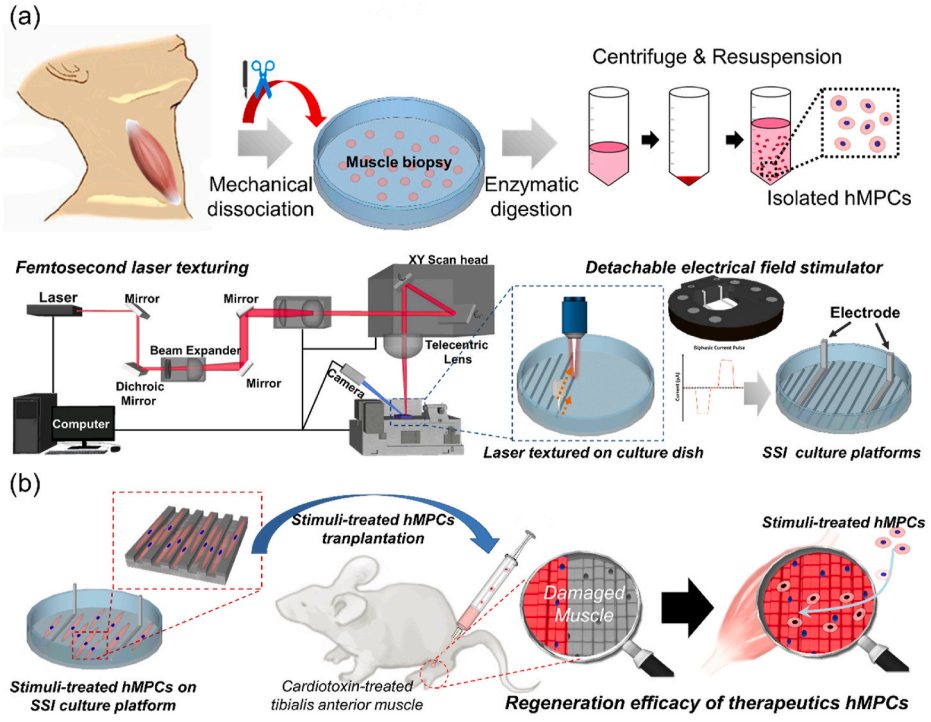

Fig. 1. (a) Schematic of isolated human muscle precursor cells (hMPCs) from human infrahyoid muscles and stimuli-treated hMPCs as potential candidates for cellular therapy. Simultaneous stimulation induction culture platform (SSI platform) with defined electrical fields and surface topography can be used to regulate the fate of hMPCs with high-regeneration efficacy. (b) Schematic diagram of the transplantation of stimuli-treated hMPCs into cardiotoxin (CTX)-treated muscle for evaluation of regeneration efficiency.

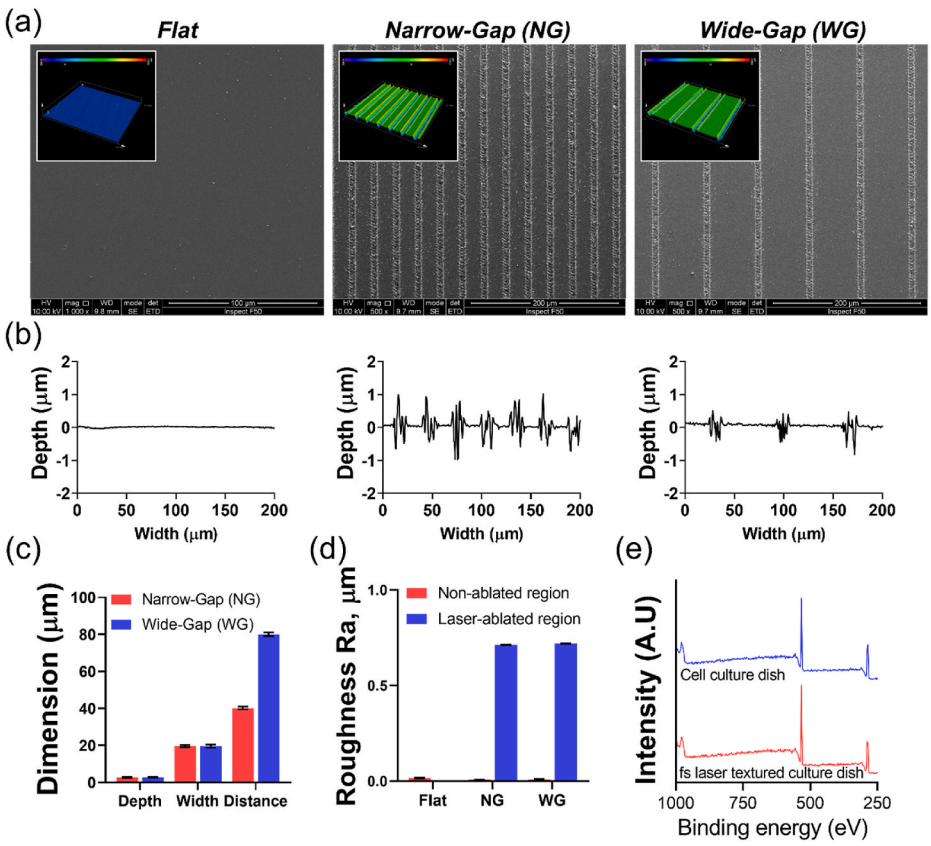

Fig. 2. Characterization of laser textured culture dishes with defined topographies textured by a femtosecond laser. A pulse duration of 400 fs and a pulse repetition rate of 500 kHz were used. The pulse scanned at a rate of 1000 mm/s to fabricate groove patterns on culture dishes. (a) Representative scanning electron microscopy (SEM) images of laser textured culture dishes. The inset in (a) shows three-dimensional (3D) imaging of laser textured culture dishes using 3D laser confocal scanning microscopy. (b) The spatial intensity profile as a function of depth was generated and obtained by 3D laser confocal scanning microscopy in the horizontal direction, which matched the direction of the underlying laser textured topographies. Quantification of laser textured (c) dimension (depth, width, and interval distance of textured topography) and (d) surface roughness of the laser textured culture dishes. (e) X-ray photoelectron spectra (XPS) of culture dishes before and after laser texturing used to affect the chemical transition process.

highest contact angle was observed in the Flat, followed by WG and NG (Supporting Information S7) cases. Wettability is known to correlate with protein adsorption and correspondingly with cell adhesion. It has been reported that wettability is mainly regulated by the surface topography and chemicals [46]. Laser-texturing can be used to transform surfaces into hydrophobic or hydrophilic characteristics by appropriately adjusting the processing parameters [47]. As such, the current laser-texturing conditions are defined based on the hydrophilicity of the culture dish surface, but it is possible to induce hydrophobicity of the culture dish surface according to the processing conditions.

3.3. Behavior of adherent cells in the SSI platform

We previously investigated and determined the optimal conditions for the viability of hMPCs based on screening at various electrical stimulation conditions (Supporting Information S8–11). Electrical stimulation conditions at 50 mV/mm did not affect the survival rate of hMPCs, even if stimulation was required for a relatively long time (Supporting Information S12). The adherent cell morphology has been demonstrated to be controllable depending on the surface topographies formed by femtosecond laser processing. As shown in Fig. 3a–c, there is

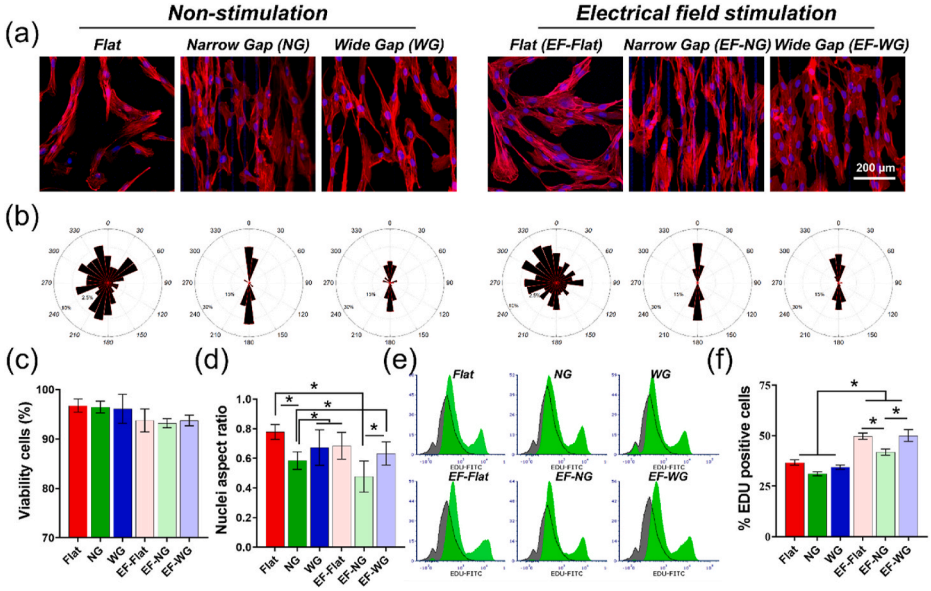

Fig. 3. Effect of the simultaneous stimulation induction culture platform (SSI platform) on the adhesion and behaviors of hMPCs. (a) Cytoskeletal structure and morphology of hMPCs on the SSI platform at 24 h. (b) Distribution of the degree of the orientation of adherent nuclei for hMPCs cultured on SSI platforms and correspondence to the 4′,6′-diamino-2-phenylindole staining results. (c) Viability for SSI platforms with or without electrical stimulation and topographies. (d) Quantification analysis of nuclear aspect ratio on SSI platforms. (e) FACS results of hMPC proliferation after 24 h of culture on SSI platforms. (f) Average % of proliferation positive cells obtained from FACS analysis of 5-ethynyl-2-deoxyuridine (EDU)-positive hMPCs. * indicates significant difference ($p < 0.05$, $n = 5$).

no specific directionality in the adherent hMPCs morphology cultured on Flat. The hMPCs on NG exhibited alignment in the direction of the laser-textured groove patterns on culture dishes. However, the hMPCs on WG did not yield directed orientation patterns, even though the cells seeded in the textured grooves exhibited aligned morphological characteristics. The same trend was observed after electrical field stimulation. Interestingly, this yielded a higher proliferative capacity in the groups subjected to electrical stimulation (Fig. 3e and f).

3.4. Effect of myogenic progenitor state in growth media

The paired-box protein (Pax7) is a prerequisite for the normal function of satellite cells during regenerative myogenesis [48]. Recent transplantation studies have indicated that stem cells that express Pax7 represent a versatile cell source for treating muscle disorders and age-associated muscle dysfunction [49,50]. Several studies have demonstrated the capacity to expand and isolate myogenic precursor cells *in vitro* [51]. However, examining the precursor potential during this expansion period revealed a steady decline in Pax7 expression, which began at values > 95% and decreased to approximately 70% by the fourth passage (Fig. 4a–c). Pax7-positive nuclei were more clearly displayed in the EF-stimulated hMPCs than in the nonstimulated hMPCs. However, there was no effect on the surface topographies between the EF-stimulated and nonstimulated cells. Consistent with the immunofluorescence results, it was proven that the Pax7-positive cells detected via flow cytometry differed depending on the electrical stimulation condition. As shown in Fig. 4b and c, the percentages of Pax7-positive nuclei among the total nuclei yielded no significant differences among the nonstimulated cells; these were 69.85 ± 4.27, 70.13 ± 3.31, and 67.47 ± 4.70% for Flat, NG, and WG, respectively. Conversely, we demonstrated that, in the EF-stimulated cell groups, the percentage of Pax7-positive nuclei was maintained at a high ratio compared with that of the freshly isolated hMPCs from muscle tissue (Supporting Information S10). These results suggest that EF stimulation can support sustained quiescent proliferative satellite cells and can provide more opportunities for them to proliferate to mature muscle cells. Evidence shows that the suitable platform for regulating cellular behaviors depends on the target tissue-specific extracellular matrix environment [52,53]. However, there is still some doubt as to whether structural and electrical characteristics affect myogenic precursor cells in simultaneous stimulation environments. As shown in Fig. 4d and e, the levels of the HSP-70 were upregulated in the EF-stimulated cells compared with that in the nonstimulated cells (Fig. 4d and e). This phenomenon induced by the electric field is partially related to the increase in the expression of the HSP. Heat stress can promote the proliferation and differentiation of muscle cells *in vitro* and enhance their regenerative potential, thus stimulating the regrowth of defected muscle tissue [54,55]. The overwhelming evidence suggests that HSPs have multiple functions in apoptosis, which in most cases lead to the inhibition of apoptotic pathways [56]. In this study, we found that the apoptotic rate of hMPCs was decreased in the cell group in which the electrical field (≤50 mV/mm) was applied (Supporting Information S9). Although there is a possibility that heat stress induced by a higher electric field can damage cells, we used the optimal electric field stimulation to minimize cell damage and prevent apoptosis. It has been reported that highly expressed HSP improves the survival rate of transplanted cells, and eventually enhances the tissue repair capability of transplanted cells [56,57]. In addition, numerous studies indicate that HSP plays an essential role in regulating the cell cycle (G1/S and S phases) [58]. As shown in Fig. 4f, the DNA contents of the EF-stimulated hMPCs were greater than those of the nonstimulated cells. These observations suggest that electric field stimulation can modulate the behavior of hMPCs more distinctly than topographical stimulation.

3.5. Effect of myogenic differentiation in differentiation medium

MRFs are basic helix-loop-helix (bHLH) transcription factors consisting of Myf-5, MyoD, and myogenin. The expression of MRF is one of the critical factors needed for the induction of skeletal muscle differentiation [59]. Based on numerous prior studies, it has been reported that quiescent satellite cells do not express detectable MRFs [60,61]. To clarify the myogenic differentiation capacity of hMPCs, we compared the expressions of MyoD, Myf5, myogenin, and MHC at various differentiation conditions. Fig. 5 shows that Myf-5 did not exhibit any significant differences according to the surface topography without EF. However, MyoD revealed higher expressions in cells cultured in NG, which can induce cellular directionality compared with other cell groups (Flat and WG). For example, the percentage changes of Myf-5 positive cells were 37.25 ± 5.13, 39.16 ± 5.86, and 37.68 ± 4.73 for Flat, NG, and WG, respectively. Conversely, the percentages of MyoD-positive nuclei on NG were 2.89 ± 0.86 and 1.84 ± 0.55 times greater than those on Flat and WG, respectively. These levels on the NG were comparable with those observed on EF-flat. These results indicate that the MRFs can be regulated depending on the topographies of the surface in contact with the cells. The EF-stimulated hMPCs yielded higher expressions of MyoD and Myf5 compared with those of the nonstimulated hMPCs. As shown in Fig. 5, we demonstrated that the expressions of MyoD and Myf5 increased markedly in the case of hMPCs

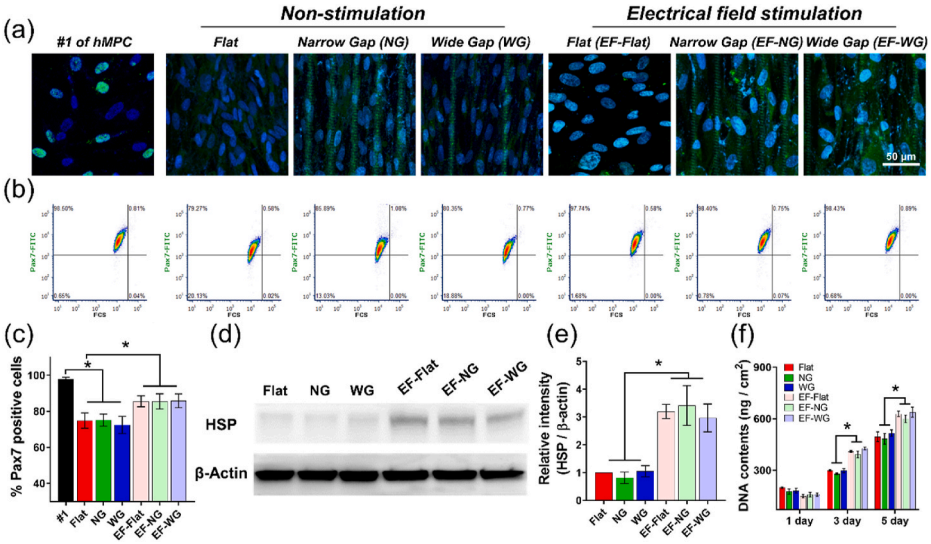

Fig. 4. (a) Representative images from isolated and cultured hMPCs and following reactions with antibodies for Pax7 on SSI platforms. (b) Flow cytometry dot plots showing expressions of Pax7 from the hMPCs cultured on SSI platforms at 3 days after culture. (c) Average numbers (%) of Pax7-positive cells obtained from FACS analysis. (d) Representative images of Western blots for anti-heat shock protein (HSP) and β-actin, and (e) the relative intensity of HSP. (f) Quantification of deoxyribonucleic acid contents. * indicates significant difference ($p < 0.05$, $n = 3$).

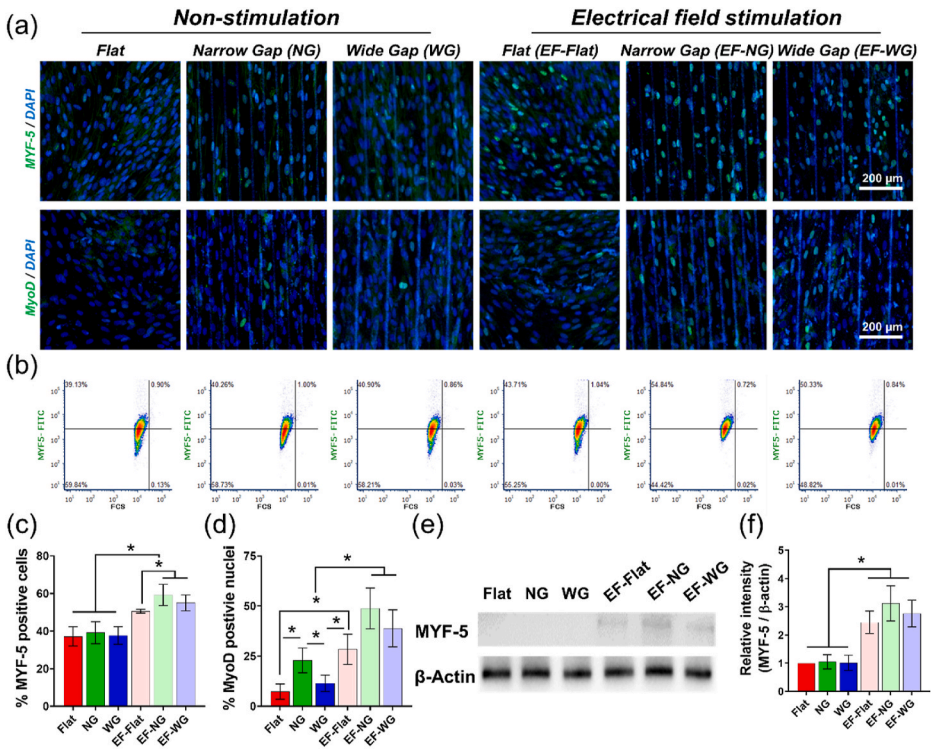

Fig. 5. (a) Representative immunofluorescence images from differentiated hMPCs on SSI platforms, reacted with antibodies for MYF-5 and MyoD for 3 days in a myogenic differentiation medium. (b) Flow cytometry dot plots showing expressions of Myf5 from the differentiated hMPCs on SSI platforms at 3 day. (c) Average % of Myf5-positive cells obtained from FACS analysis. (d) MyoD-positive nuclei percentage on the SSI platforms. (e) Representative images of Western blots for Myf5 and β-actin, and (f) the relative intensity of Myf5. * indicates significant difference ($p < 0.05$, $n = 5$).

cultured on surfaces with oriental surface topography. In addition, it was confirmed that the expression of myogenic regulators in myogenic precursor cells yielded a synergistic effect in simultaneous topographic and electrical stimulation conditions.

Quiescent mononucleated myogenic cells become activated during myogenic differentiation [62]. The serial event includes the over-expression of several differentiation markers, such as myogenin and fusion, to form multinucleated myofibers with the expression of MHC. The qualitative and quantitative analysis of myogenin with the use of an immunofluorescent microscope validated these outcomes (Fig. 6a and Supporting Information S14). In addition, multinucleated myoblasts (also known as myotubes) are interpreted and utilized as initial building blocks for skeletal muscle regeneration. Consistent with other results, we confirmed that the hMPCs cultured on the laser-textured cultured dishes (NG and WG) proceeded to differentiate in an anisotropic myotube assembly (Fig. 6). The distribution of the myotube orientation was <15° relative to the NG and WG, whereas a broader distribution was observed on Flat. These observations suggest that the surface topographies aid in the orientation of the myotube assembly, but the effect of myogenic differentiation is more dominant with electrical stimulation.

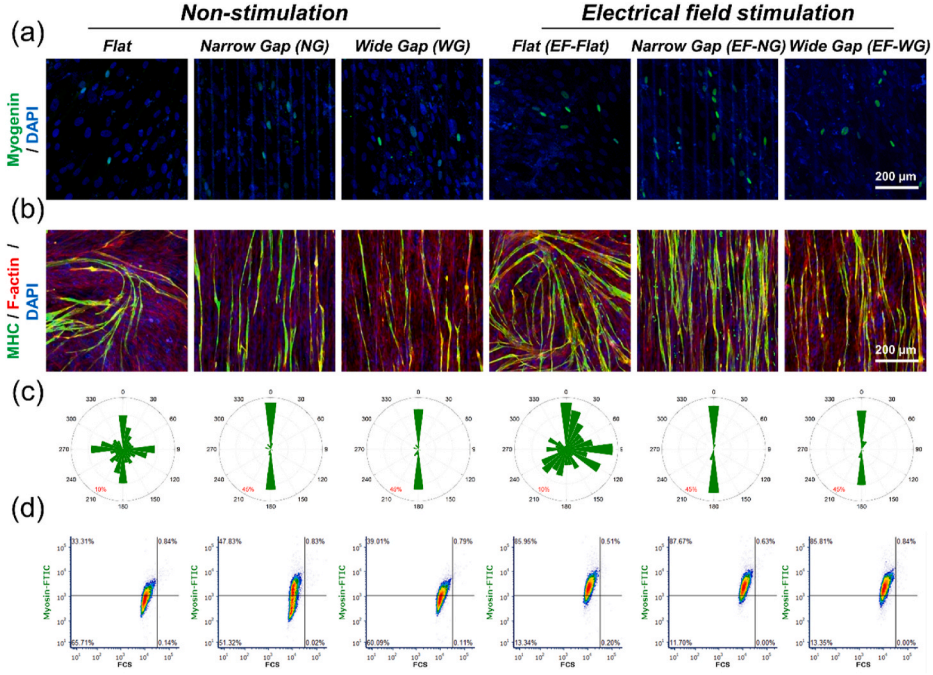

Fig. 6. (a) Representative immunofluorescence images of myogenin-positive hMPCs cultured on SSI platforms for 7 days in a myogenic differentiation medium. (b) Representative immunofluorescence images of sarcomeric myosin heavy chain-positive (MHC)-positive hMPCs cultured on SSI platforms for 14 days in a myogenic differentiation medium. (c) Distribution of myotube orientation corresponding to MHC-positive hMPCs. (d) Flow cytometry dot plots showing expressions of sarcomeric myosin heavy chain (Myosin) from the differentiated hMPCs on SSI platforms at day 14.

This is demonstrated in Fig. 6d, which shows a higher relative abundance of MHC-positive cells in the EF groups. The expressions of MHC were 39.30 ± 3.93, 51.13 ± 5.56, 43.97 ± 4.27, 67.32 ± 5.39, 82.19 ± 4.34, and 73.18 ± 2.31 for Flat, NG, WG, EF-flat, EF-NG, and EF-WG, respectively (Supporting Information S15). Our results suggest that our SSI platform can be used to achieve the desired shape and myogenic function of hMPCs in a cultural environment that simultaneously provides both topographical and electrical stimuli. These findings indicate that the laser technology on commercially available plastic culture ware may serve as a potential universal culture platform *in vitro*. In addition to the nonconductive culture dish used, conductive materials are an effective culture platform used to replicate the electrical and biological characteristics of tissues requiring conductivity. We previously demonstrated that femtosecond laser technology could be applied to various biomaterials [20,21,63,64]. Even in the case of hydrogels, in addition to cell culture plasticware, we demonstrated that the orientation of hMPCs could be induced via femtosecond laser texturing in ECM-coated polyacrylamide (PA) hydrogels (Supporting Information S16). Our future studies will focus on the synergistic effect of myogenic progenitor cells on easily accessible conductive/nonconductive culture platforms on adherent orientation, differentiation, and muscle regeneration following EF stimulation.

3.6. Regeneration potential of hMPCs

The regeneration potential of hMPCs stimulated from topographical and electrical stimuli was evaluated in the mouse model. The TA muscles of athymic mice were injured by CTX injections. Cardiotoxin (CTX)-induced muscle injury models, with their combination of rapid recovery time and localized damage, are ideal for solving the mechanistic and molecular aspects of skeletal muscle regeneration [65,66]. In addition, the CTX severely destroys muscle fibers but does not entirely damage the extracellular matrix (ECM) and satellite cells (i.e., Pax7 expression), thus enabling tissue regeneration (Supporting Information S17) [67,68]. After 24 h following CTX injection, the hMPCs were infused in the injured TA muscles. Seven cell groups were compared: the uninjured (normal group), CTX injured (no-treatment group), and saline-treated CTX injured TA muscles (saline-treated group) without cell infusion served as the control groups, while the injection of hMPCs from Flat, NG, EF-flat, and EF-NG served as the experimental groups. Two weeks after the cell transplant, the excised TA muscles were stained with H&E and MT to examine the cross-sectional morphologies of the myofibers (Supporting Information S18). In the no-treatment and saline-treated groups, most of the myofibers degenerated, and numerous fate depositions with extensive fibrosis were observed. A small number of myofibers with the nuclei located at the center of the myofiber observed in the group injecting hMPCs obtained from a Flat and NG. When EF-stimulated hMPCs were transplanted, degenerating myofibers were rarely found, and the centrally nucleated regenerating myofibers represented the majority in the muscle tissue. It was also found that the intramuscular injection of electrically stimulated hMPCs had a tissue-protective effect and led to a reduction in the necrotic span. However, our results demonstrated a diminished therapeutic effect with the nonstimulated groups compared with the EF-stimulated groups, thus suggesting that transplantation of cells without external stimulation is not sufficient to maximize the regenerative impact. Therefore, the primary aim of this study was the validation of the therapeutic effects of hMPC and the investigation of the enhanced muscle regeneration efficacy of transplanted cells following external stimulation. Human nuclear staining confirmed the presence of engrafted hMPCs (yellow arrows in Fig. 7a). Analysis of the HNA-positive cells transplanted in the muscle with the use of flow cytometry validated these outcomes (Fig. 7b). These results indicated that progressive tissue regeneration was manifested in a large number of dystrophic muscle fibers, along with the integration of myogenic cells at the injured muscle site. We also conducted an immunohistochemical analysis of laminin in the CTX-induced TA muscle (Fig. 7a). Laminin is a strongly expressed ECM protein in the basement membrane of skeletal muscle [69]. The transplanted hMPCs obtained from the EF-flat and EF-NG groups displayed higher laminin expressions, and the shape of laminin matched the myofiber shape. The myogenic factor Myf5 defines the onset of myogenesis in mammals during development [70]. In addition, it has been demonstrated that muscle regeneration from satellite cells is mainly based on the finding that proliferating and differentiating satellite cells re-express myogenic regulatory factors (MyoD, Myf5, Myogenin, and Myf6) [6]. To confirm the role of the transplanted cells, flow cytometry of HNA+/Myf5+ was conducted (Fig. 7c). Double staining with HNA and Myf5 confirmed that the delivered cells participated in the muscle regeneration process. The relative quantity of the HNA+/Myf5+ cells was similar for the EF groups (2.89% for EF-flat and 3.79% for EF-NG), but the differences with nonstimulated cells groups were nearly five-fold (0.44% for Flat and 0.71% for NG). Thus, the stimulated hMPC population yielded a higher HNA+/Myf5+ expression ratio than the nonstimulated cells, providing additional evidence for the regenerative capacity of the transplanted cell population. Staining against MHC and laminin revealed the extensive formation of new MHC-positive

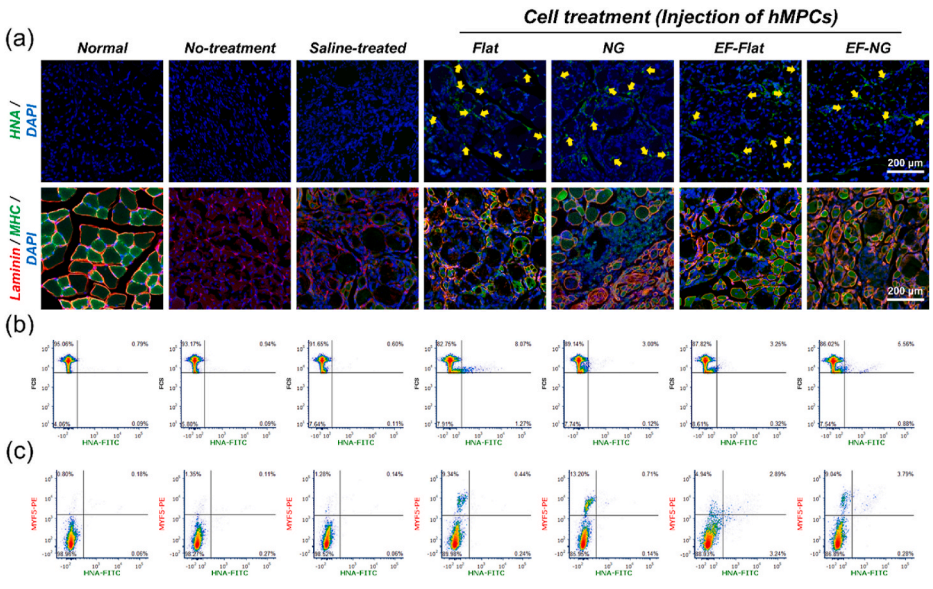

Fig. 7. Transplantation of hMPCs impaired skeletal muscle mouse model. Normal (uninjured skeletal muscle), No-treatment (CTX treated muscle), Saline-treated (saline injection (20 μL) into CTX-treated muscle), Cell treatment (injection of hMPCs (1.5×10^5 cells in 20 μL) from cultured SSI-platforms into CTX treated muscle. (a) Representative images of immunofluorescence staining (Laminin, and human nuclear antigen (HNA)) of tibialis anterior (TA) muscle 14 days after hMPCs transplantation. (b) Flow cytometry dot plots showing expression of HNA from the collected hMPCs transplanted into TA muscle at 14 day. (c) Flow cytometry dot plots showing expressions of HNA and Myf5 from the collected hMPCs transplanted into the TA muscle at day 14. HNA was indicated by yellow arrows. (For interpretation of the references to colour in this figure legend, the reader is referred to the Web version of this article.)

myofibers with correct laminin deposition when EF-stimulated hMPCs were transplanted. These results suggest that the physically and electrically stimulated hMPCs can perform their roles as myogenic precursor cells after transplantation in injured muscle tissue. Coupling angiogenesis and myogenesis are critical for the long-term functional restoration of an injured muscle [71]. To assess vascular density, muscle tissue sections were stained by specific antibodies against SMA and CD31. It was confirmed that capillary and arteriolar densities were found in the EF-stimulated hMPC groups, as compared with those in the other groups (Fig. 8). All cell-treated groups had a higher number of CD31 positive capillaries in the newly formed tissues than those of untreated control. Specifically, the most significant increase in capillary density was observed in the EF-stimulated hMPC groups. Our results show that the coupling ratio between angiogenesis and myogenesis is more elevated than that of group nonstimulated cells when the stimulated-hMPCs are transplanted into the damaged muscle area. The relative quantities of the CD31+/MYH + cells were similar in both EF groups (3.80% for EF-flat and 5.00% for EF-NG), but the differences with nonstimulated cells groups were nearly four-fold (0.59% for Flat and 1.11% for NG). Despite the fact that we could not confirm the comparison with HNA in all *in vivo* results, HNA+/Myf5+ and CD31+/MYH + results proved that the transplanted hMPCs around the damaged muscle were regenerated. Collectively, these results indicate that the EF-stimulated hMPCs yield the highest regenerative capability at 2 weeks post-injury. Furthermore, it was confirmed that the hMPCs that experienced electrical stimulation through the laser texture topography promoted muscle regeneration as a cell source with a therapeutic effect. Therefore, we can conclude that the hMPCs obtained using SSI platforms are appropriate and preferable types of therapeutic cells for muscle regeneration. Although in this study (at the proof-of-concept stage) the hMPCs from the SSI platforms were directly transplanted into the damaged muscle, we believe that transplanting the cells using biomaterial-based carriers (such as collagen, gelatin, or fibrin gels) is more appropriate from the standpoint of cell delivery. Therefore, a follow-up study is intended to be conducted to investigate the regenerative muscle effects of functionalized hMPCs on SSI platforms using a carrier during tissue transplantation.

4. Conclusions

Our results suggest that surface topography determines the direction of adherent hMPCs compared with electrical field stimulation. Electrical field stimulation had an appreciable effect on myogenic differentiation. Laser-textured groove patterns enhanced the orientation and elongation along the groove direction, but could not reverse the effects of the cues provided by electrical stimulation. The myogenesis of hMPCs on the laser-textured surfaces and following electrical field stimulation represented a completely enhanced myogenic differentiation response. We used the CTX-induced mouse model to demonstrate that the EF-stimulated hMPC transplantation led to considerably higher myogenesis and perfusion restoration responses than those after untreated cell administration. Our study highlights the importance of the presentation of simultaneous, biologically relevant cues to study myogenic differentiation processes, and indicates that stimuli-treated hMPC transplantations may play a significant role in the regeneration of injured muscle. Our results indicate the beneficial effects of stimuli based on *in vitro* cell culture platforms capable of obtaining therapeutically efficient human cells for muscle recovery in a mouse injury model similar to muscle lesions. These findings have profound implications for the design of *in vitro* culture platforms for tissue engineering.

CRediT authorship contribution statement

Indong Jun: Conceptualization, Investigation, Formal analysis, Methodology, Visualization, Writing – original draft, Writing – review & editing. **Na Li:** Formal analysis, Methodology, Visualization. **Jaeho Park:** Formal analysis. **Young Jun Kim:** Investigation, Supervision.

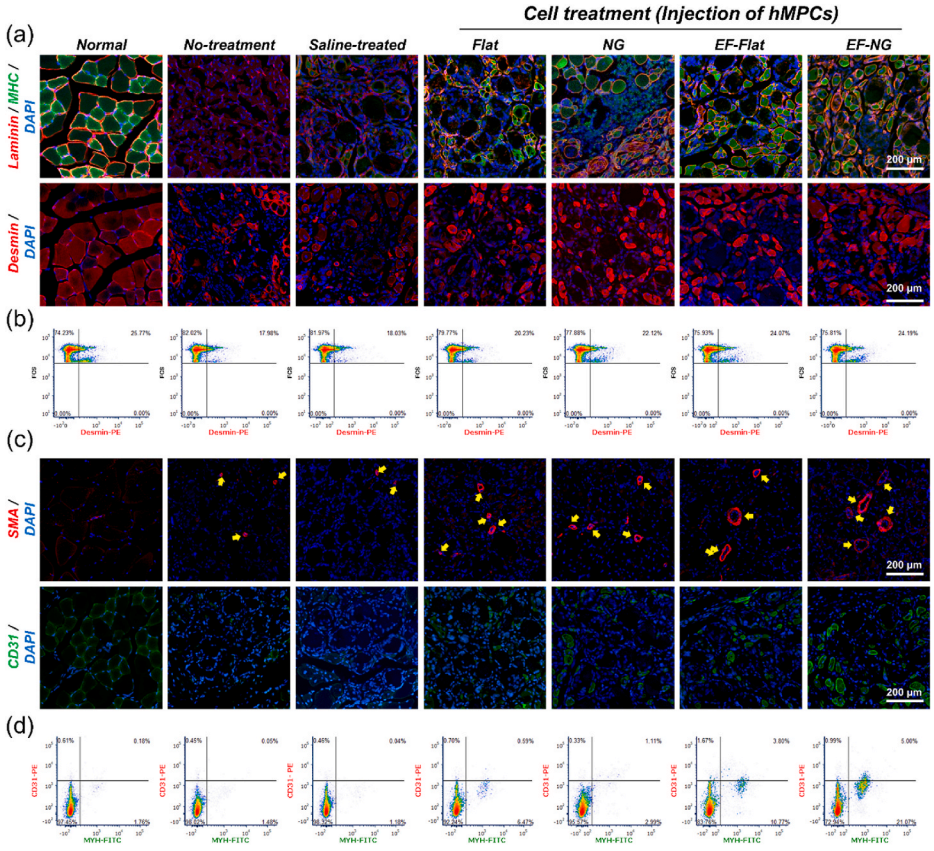

Fig. 8. Therapeutic and angiogenic effects of transplanted hMPCs in an impaired skeletal muscle mouse model. (a) Representative images of immunofluorescence staining (MHC and Desmin) of the tibialis anterior (TA) muscle 14 days after hMPCs transplantation. (b) Flow cytometry dot plots showing expression of desmin from the transplanted hMPCs into the TA muscle at day 14. (c) Representative images of immunofluorescence staining (SMA and CD31 (PECAM)) of tibialis anterior (TA) muscle 14 days after hMPCs transplantation. (d) Flow cytometry dot plots showing expression of CD31 and MYH from the transplanted hMPCs into TA muscle at 14 day. Arteriole formation (SMA-positive vessel) was indicated by yellow arrows. (For interpretation of the references to colour in this figure legend, the reader is referred to the Web version of this article.)

Hojeong Jeon: Investigation, Supervision. **Hyuk Choi:** Investigation, Supervision. **Jae-Gu Cho:** Investigation, Methodology, Supervision. **Byoung Chan Choi:** Investigation, Methodology, Resources, Supervision. **Hyung-Seop Han:** Conceptualization, Funding acquisition, Writing – review & editing. **Jae-Jun Song:** Funding acquisition, Project administration, Supervision.

Declaration of competing interest

The authors declare no conflict of interest.

Acknowledgements

This work was supported by a Korean National Research Foundation (NRF) grant funded by the Korea government (MSIT) (No. 2017M3A9G1027929). It was also supported by both the National Research Council of Science & Technology 424 (NST) grant by the Korean government (MSIP) (CAP-17-01-KIST Europe) and KIST project (2E31121).

Appendix A. Supplementary data

Supplementary data to this article can be found online at https://doi.org/10.1016/j.bioactmat.2021.10.015.

References

[1] T.H. Qazi, G.N. Duda, M.J. Ort, C. Perka, S. Geissler, T. Winkler, Cell therapy to improve regeneration of skeletal muscle injuries, J. Cachexia Sarcopenia Muscle 10 (3) (2019) 501–516.
[2] S.E. Berry, Concise review: mesoangioblast and mesenchymal stem cell therapy for muscular dystrophy: progress, challenges, and future directions, Stem Cells Transl. Med. 4 (1) (2015) 91–98.
[3] M.H. Parker, S.J. Tapscott, Expanding donor muscle-derived cells for transplantation, Curr. Protoc. Stem Cell Biol. Chapter 2 (2013). Unit 2C 4.
[4] D. Skuk, J.P. Tremblay, The process of engraftment of myogenic cells in skeletal muscles of primates: understanding clinical observations and setting directions in cell transplantation research, Cell Transplant. 26 (11) (2017) 1763–1779.
[5] N.A. Dumont, C.F. Bentzinger, M.C. Sincennes, M.A. Rudnicki, Satellite cells and skeletal muscle regeneration, Comp. Physiol. 5 (3) (2015) 1027–1059.
[6] H. Yin, F. Price, M.A. Rudnicki, Satellite cells and the muscle stem cell niche, Physiol. Rev. 93 (1) (2013) 23–67.
[7] B. Langridge, M. Griffin, P.E. Butler, Regenerative medicine for skeletal muscle loss: a review of current tissue engineering approaches, J. Mater. Sci. Mater. Med. 32 (1) (2021) 15.
[8] A. Magli, R.R.C. Perlingeiro, Myogenic progenitor specification from pluripotent stem cells, Semin. Cell Dev. Biol. 72 (2017) 87–98.
[9] M.H. Parker, Assaying human myogenic progenitor cell activity by reconstitution of muscle fibers and satellite cells in immunodeficient mice, Methods Mol. Biol. 1460 (2016) 209–221.
[10] M. Buckingham, Myogenic progenitor cells and skeletal myogenesis in vertebrates, Curr. Opin. Genet. Dev. 16 (5) (2006) 525–532.
[11] B. Mierzejewski, K. Archacka, I. Grabowska, A. Florkowska, M.A. Ciemerych, E. Brzoska, Human and mouse skeletal muscle stem and progenitor cells in health and disease, Semin. Cell Dev. Biol. 104 (2020) 93–104.
[12] A.S. Mao, D.J. Mooney, Regenerative medicine: current therapies and future directions, Proc. Natl. Acad. Sci. U. S. A. 112 (47) (2015) 14452–14459.
[13] N. Rosenthal, S. Badylak, Regenerative medicine: today's discoveries informing the future of medical practice, NPJ Regen. Med. 1 (2016), 16007.
[14] M.J. Lerman, J. Lembong, S. Muramoto, G. Gillen, J.P. Fisher, The evolution of polystyrene as a cell culture material, Tissue Eng. B Rev. 24 (5) (2018) 359–372.
[15] K.H. Nakayama, M. Shayan, N.F. Huang, Engineering biomimetic materials for skeletal muscle repair and regeneration, Adv. Healthc Mater. 8 (5) (2019), e1801168.
[16] S. Jana, S.K. Levengood, M. Zhang, Anisotropic materials for skeletal-muscle-tissue engineering, Adv Mater. 28 (48) (2016) 10588–10612.
[17] J. Pruller, I. Mannhardt, T. Eschenhagen, P.S. Zammit, N. Figeac, Satellite cells delivered in their niche efficiently generate functional myotubes in three-dimensional cell culture, PLoS One 13 (9) (2018), e0202574.
[18] J. Chal, O. Pourquie, Making muscle: skeletal myogenesis in vivo and in vitro, Development 144 (12) (2017) 2104–2122.
[19] A.M. Almonacid Suarez, Q. Zhou, P. van Rijn, M.C. Harmsen, Directional topography gradients drive optimum alignment and differentiation of human myoblasts, J. Tissue Eng. Regen. Med. 13 (12) (2019) 2234–2245.
[20] I. Jun, Y.W. Chung, Y.H. Heo, H.S. Han, J. Park, H. Jeong, H. Lee, Y.B. Lee, Y. C. Kim, H.K. Seok, H. Shin, H. Jeon, Creating hierarchical topographies on fibrous platforms using femtosecond laser ablation for directing myoblasts behavior, ACS Appl. Mater. Interfaces 8 (5) (2016) 3407–3417.
[21] I. Jun, Y.W. Chung, J. Park, H.S. Han, J. Park, S. Kim, H. Lee, S.H. Kim, J.H. Han, H. Kim, H.K. Seok, Y.C. Kim, H. Jeon, Ultrathin metal films with defined topographical structures as in vitro cell culture platforms for unveiling vascular cell behaviors, Adv. Healthc Mater. 5 (18) (2016) 2396–2405.
[22] I. Jun, S.J. Kim, E. Choi, K.M. Park, T. Rhim, J. Park, K.D. Park, H. Shin, Preparation of biomimetic hydrogels with controlled cell adhesive properties and topographical features for the study of muscle cell adhesion and proliferation, Macromol. Biosci. 12 (11) (2012) 1502–1513.
[23] W. Kim, C.H. Jang, G.H. Kim, A myoblast-laden collagen bioink with fully aligned Au nanowires for muscle-tissue regeneration, Nano Lett. 19 (12) (2019) 8612–8620.
[24] B. Maleiner, J. Tomasch, P. Heher, O. Spadiut, D. Runzler, C. Fuchs, The importance of biophysical and biochemical stimuli in dynamic skeletal muscle models, Front. Physiol. 9 (2018) 1130.
[25] C. Handschin, A. Mortezavi, J. Plock, D. Eberli, External physical and biochemical stimulation to enhance skeletal muscle bioengineering, Adv. Drug Deliv. Rev. 82–83 (2015) 168–175.
[26] A. Kumar, J.K. Placone, A.J. Engler, Understanding the extracellular forces that determine cell fate and maintenance, Development 144 (23) (2017) 4261–4270.
[27] B. Ferrigno, R. Bordett, N. Duraisamy, J. Moskow, M.R. Arul, S. Rudraiah, S. P. Nukavarapu, A.T. Vella, S.G. Kumbar, Bioactive polymeric materials and electrical stimulation strategies for musculoskeletal tissue repair and regeneration, Bioact. Mater. 5 (3) (2020) 468–485.
[28] A. Patel, S. Vendrell-Gonzalez, G. Haas, M. Marcinczyk, N. Ziemkiewicz, M. Talovic, J.S. Fisher, K. Garg, Regulation of myogenic activity by substrate and electrical stimulation in vitro, Biores. Open Access 8 (1) (2019) 129–138.
[29] R.A. Vadlamani, Y. Nie, D.A. Detwiler, A. Dhanabal, A.M. Kraft, S. Kuang, T. P. Gavin, A.L. Garner, Nanosecond pulsed electric field induced proliferation and differentiation of osteoblasts and myoblasts, J. R. Soc. Interface 16 (155) (2019), 20190079.
[30] H.S. Yang, B. Lee, J.H. Tsui, J. Macadangdang, S.Y. Jang, S.G. Im, D.H. Kim, Electroconductive nanopatterned substrates for enhanced myogenic differentiation and maturation, Adv. Healthc Mater. 5 (1) (2016) 137–145.
[31] U.H. Ko, S. Park, H. Bang, M. Kim, H. Shin, J.H. Shin, Promotion of myogenic maturation by timely application of electric field along the topographical alignment, Tissue Eng. 24 (9–10) (2018) 752–760.
[32] Y. Jin, D. Shahriari, E.J. Jeon, S. Park, Y.S. Choi, J. Back, H. Lee, P. Anikeeva, S. W. Cho, Functional skeletal muscle regeneration with thermally drawn porous fibers and reprogrammed muscle progenitors for volumetric muscle injury, Adv Mater. 33 (14) (2021), e2007946.
[33] M.F. Pittenger, D.E. Discher, B.M. Peault, D.G. Phinney, J.M. Hare, A.I. Caplan, Mesenchymal stem cell perspective: cell biology to clinical progress, NPJ Regen. Med. 4 (2019) 22.
[34] A. Deganello, C.R. Leemans, The infrahyoid flap: a comprehensive review of an often overlooked reconstructive method, Oral Oncol. 50 (8) (2014) 704–710.
[35] H.S. Lee, S.W. Kim, H.S. Park, C.W. Park, J.S. Kim, J.C. Hong, Y.K. Kim, S.M. Baek, K.D. Lee, Partial cutting of sternothyroid muscle during total thyroidectomy: impact on postoperative vocal outcomes, Sci. World J. 2013 (2013), 416535.
[36] D. Eberli, S. Soker, A. Atala, J.J. Yoo, Optimization of human skeletal muscle precursor cell culture and myofiber formation in vitro, Methods 47 (2) (2009) 98–103.
[37] J.H. Kim, H. Choi, M.J. Suh, J.H. Shin, M.H. Hwang, H.M. Lee, Effect of biphasic electrical current stimulation on IL-1β-stimulated annulus fibrosus cells using in vitro microcurrent generating chamber system, Spine (Phila Pa 38 (22) (2013) E1368–E1376, 1976.
[38] D. Montarras, J. Morgan, C. Collins, F. Relaix, S. Zaffran, A. Cumano, T. Partridge, M. Buckingham, Direct isolation of satellite cells for skeletal muscle regeneration, Science 309 (5743) (2005) 2064–2067.
[39] H. Yin, F. Price, M.A. Rudnicki, Satellite cells and the muscle stem cell niche, Physiol. Rev. 93 (1) (2013) 23–67.
[40] O. Bar-Nur, M.F.M. Gerli, B. Di Stefano, A.E. Almada, A. Galvin, A. Coffey, A. J. Huebner, P. Feige, C. Verheul, P. Cheung, D. Payzin-Dogru, S. Paisant, A. Anselmo, R.I. Sadreyev, H.C. Ott, S. Tajbakhsh, M.A. Rudnicki, A.J. Wagers, K. Hochedlinger, Direct reprogramming of mouse fibroblasts into functional skeletal muscle progenitors, Stem Cell Rep. 10 (5) (2018) 1505–1521.
[41] A. Riveiro, A.L.B. Maçon, J. del Val, R. Comesaña, J. Pou, Laser surface texturing of polymers for biomedical applications, Front. Phys. 6 (2018) 16.
[42] I. Shivakoti, G. Kibria, R. Cep, B.B. Pradhan, A. Sharma, Laser surface texturing for biomedical applications: a review, Coatings 11 (2) (2021) 124.
[43] H. Jeon, S. Koo, W.M. Reese, P. Loskill, C.P. Grigoropoulos, K.E. Healy, Directing cell migration and organization via nanocrater-patterned cell-repellent interfaces, Nat. Mater. 14 (9) (2015) 918–923.
[44] A. Daskalova, A. Selimis, A. Manousaki, D. Gray, A. Ranella, C. Fotakis, Surface modification of collagen-based biomaterial induced by pulse width variable femtosecond laser pulses, SPIE 8770 (2013).
[45] M.E. Kavousanakis, N.T. Chamakos, A.G. Papathanasiou, Connection of intrinsic wettability and surface topography with the apparent wetting behavior and adhesion properties, J. Phys. Chem. C 119 (27) (2015) 15056–15066.
[46] B. Majhy, P. Priyadarshini, A.K. Sen, Effect of surface energy and roughness on cell adhesion and growth – facile surface modification for enhanced cell culture, RSC Adv. 11 (25) (2021) 15467–15476.
[47] A. Riveiro, P. Pou, J. del Val, R. Comesaña, F. Arias-González, F. Lusquiños, M. Boutinguiza, F. Quintero, A. Badaoui, J. Pou, Laser texturing to control the wettability of materials, Procedia CIRP 94 (2020) 879–884.

[48] J. von Maltzahn, A.E. Jones, R.J. Parks, M.A. Rudnicki, Pax7 is critical for the normal function of satellite cells in adult skeletal muscle, Proc. Natl. Acad. Sci. Unit. States Am. 110 (41) (2013) 16474–16479.
[49] M. Cerletti, S. Jurga, C.A. Witczak, M.F. Hirshman, J.L. Shadrach, L.J. Goodyear, A. J. Wagers, Highly efficient, functional engraftment of skeletal muscle stem cells in dystrophic muscles, Cell 134 (1) (2008) 37–47.
[50] B.D. Cosgrove, P.M. Gilbert, E. Porpiglia, F. Mourkioti, S.P. Lee, S.Y. Corbel, M. E. Llewellyn, S.L. Delp, H.M. Blau, Rejuvenation of the muscle stem cell population restores strength to injured aged muscles, Nat. Med. 20 (3) (2014) 255–264.
[51] B.C. Syverud, J.D. Lee, K.W. VanDusen, L.M. Larkin, Isolation and purification of satellite cells for skeletal muscle tissue engineering, J. Regen. Med. 3 (2) (2014).
[52] M. Ahmed, C. Ffrench-Constant, Extracellular matrix regulation of stem cell behavior, Curr. Stem Cell Rep. 2 (2016) 197–206.
[53] B. Yue, Biology of the extracellular matrix: an overview, J. Glaucoma 23 (8 Suppl 1) (2014) S20–S23.
[54] Q. Guo, D. Miller, H. An, H. Wang, J. Lopez, D. Lough, L. He, A. Kumar, Controlled heat stress promotes myofibrillogenesis during myogenesis, PLoS One 11 (11) (2016), e0166294.
[55] J. Tang, A. He, H. Yan, G. Jia, G. Liu, X. Chen, J. Cai, G. Tian, H. Shang, H. Zhao, Damage to the myogenic differentiation of C2C12 cells by heat stress is associated with up-regulation of several selenoproteins, Sci. Rep.-Uk 8 (1) (2018), 10601.
[56] Q. Wang, X. Li, Q. Wang, J. Xie, C. Xie, X. Fu, Heat shock pretreatment improves mesenchymal stem cell viability by heat shock proteins and autophagy to prevent cisplatin-induced granulosa cell apoptosis, Stem Cell Res. Ther. 10 (1) (2019) 348.
[57] G.C. Fan, Role of heat shock proteins in stem cell behavior, Prog. Mol. Biol. Transl. Sci. 111 (2012) 305–322.
[58] N.M. Kuhl, L. Rensing, Heat shock effects on cell cycle progression, Cell. Mol. Life Sci. 57 (3) (2000) 450–463.
[59] J.M. Hernández-Hernández, E.G. García-González, C.E. Brun, M.A. Rudnicki, The myogenic regulatory factors, determinants of muscle development, cell identity and regeneration, Semin. Cell Dev. Biol. 72 (2017) 10–18.
[60] P.S. Zammit, T.A. Partridge, Z. Yablonka-Reuveni, The skeletal muscle satellite cell: the stem cell that came in from the cold, J. Histochem. Cytochem. 54 (11) (2006) 1177–1191.
[61] J.R. Beauchamp, L. Heslop, D.S. Yu, S. Tajbakhsh, R.G. Kelly, A. Wernig, M. E. Buckingham, T.A. Partridge, P.S. Zammit, Expression of CD34 and Myf5 defines the majority of quiescent adult skeletal muscle satellite cells, J. Cell Biol. 151 (6) (2000) 1221–1234.
[62] X. Fu, H. Wang, P. Hu, Stem cell activation in skeletal muscle regeneration, Cell. Mol. Life Sci. 72 (9) (2015) 1663–1677.
[63] I. Jun, K. Kim, Y.W. Chung, H.J. Shin, H.S. Han, J.R. Edwards, M.R. Ok, Y.C. Kim, H.K. Seok, H. Shin, H. Jeon, Effect of spatial arrangement and structure of hierarchically patterned fibrous scaffolds generated by a femtosecond laser on cardiomyoblast behavior, J. Biomed. Mater. Res. 106 (6) (2018) 1732–1742.
[64] Y. Seo, S. Kim, H.S. Lee, J. Park, K. Lee, I. Jun, H. Seo, Y.J. Kim, Y. Yoo, B.C. Choi, H.K. Seok, Y.C. Kim, M.R. Ok, J. Choi, C.K. Joo, H. Jeon, Femtosecond laser induced nano-textured micropatterning to regulate cell functions on implanted biomaterials, Acta Biomater. 116 (2020) 138–148.
[65] M.A. Mahdy, H.Y. Lei, J. Wakamatsu, Y.Z. Hosaka, T. Nishimura, Comparative study of muscle regeneration following cardiotoxin and glycerol injury, Ann. Anat. 202 (2015) 18–27.
[66] G.A. Garry, M.L. Antony, D.J. Garry, Cardiotoxin induced injury and skeletal muscle regeneration, Methods Mol. Biol. 1460 (2016) 61–71.
[67] S.T. Sicherer, R.S. Venkatarama, J.M. Grasman, Recent trends in injury models to study skeletal muscle regeneration and repair, Bioengineering (Basel) 7 (3) (2020).
[68] M. Juhas, N. Abutaleb, J.T. Wang, J. Ye, Z. Shaikh, C. Sriworarat, Y. Qian, N. Bursac, Incorporation of macrophages into engineered skeletal muscle enables enhanced muscle regeneration, Nat. Biomed. Eng. 2 (12) (2018) 942–954.
[69] R. Csapo, M. Gumpenberger, B. Wessner, Skeletal muscle extracellular matrix - what do we know about its composition, regulation, and physiological roles? A narrative review, Front. Physiol. 11 (2020) 253, 253.
[70] S. Gunther, J. Kim, S. Kostin, C. Lepper, C.M. Fan, T. Braun, Myf5-positive satellite cells contribute to Pax7-dependent long-term maintenance of adult muscle stem cells, Cell Stem Cell 13 (5) (2013) 590–601.
[71] J. Gilbert-Honick, W. Grayson, Vascularized and innervated skeletal muscle tissue engineering, Adv. Healthcare Mater. 9 (1) (2020), e1900626 e1900626.